Available free online at www.medjchem.com

Mediterranean Journal of Chemistry

Mediterranean Journal of Chemistry **2023**, 13(1), 50-58

Synthesis and Characterization of Ternary Composite g-C_3N_4-MoO_3/rGO for Photocatalytic Activity

Zainab Waheed [1], Sadia Ghazanfar [1], Muhammad Usman [2], Khalid Mahmood [1], Ajaz Hussain [1], Muhammad Sirajuddin [3], and Muhammad Tariq [1,*]

[1] Institute of Chemical Sciences, Bahauddin Zakariya University, 60800, Multan, Pakistan

[2] Institute of Biomedical Materials and Engineering, College of Materials Science and Engineering, Qingdao University, 308 Ningxia Road, Qingdao, Shangdong 266071, China

[3] Department of Chemistry, University of Science & Technology, 28100 Bannu, Pakistan

Abstract: The present research prepared a ternary composite g-C3N4-MoO3/rGO using the ultrasonic-assisted wet impregnation method. The prepared photocatalyst was characterized by using Fourier transform infrared spectroscopy (FT-IR), Powder X-ray diffraction (XRD), scanning electron microscopy (SEM), and EDX(Energy dispersive X-ray) techniques. The structure and morphology of pure MoO_3, g-C_3N_4, binary composite g-C_3N_4-MoO_3, and ternary composite g-C_3N_4-MoO_3/rGO have been studied in their photocatalytic performance in the degradation of Rhodamine B (Rh-B) was tested and compared. The ternary composite g-C_3N_4-MoO_3/rGO exhibited better degradation efficiency of 80% than pure and binary composite. The synergistic effect of the three components resulted in enhanced light-capturing ability, high charge separation, and low recombination rate of electron-hole pair.

Keywords: Impregnation; Composite; Photocatalysts; Degradation; Separation; Recombination.

1. Introduction

The organic dyes from various industrial effluents have posed a severe ultimate threat to humans, aquatic macro & microorganisms, and ecological systems [1,2]. The dye-containing effluents pollute surrounding canals, rivers, and groundwater because of their increasing usage in various industries like textile, leather, paper & pulp, food, chemical, etc. [3,4]. More than ten thousand dyes have been used worldwide in the textile industry [4]. 10-20 % of dyes have been lost during the dyeing process, and 5-20 % are directly discharged into the water environment [4]. The cation dye of rhodamine B (Rh B) is the most commonly used xanthenes dye for the textile industry and is well-known for its good stability. However, Rh B can dissolve well in water or organic solvent and has been found to be potentially toxic and carcinogenic [5,6], which prevents it from being used in foods and cosmetics. Rh B is commonly used as a target pollutant in photocatalyst research about the purification of practical industrial wastewater because on entering the water streams, Rh B consumes dissolved oxygen which causes the devastation of aquatic life. Water quality reaches incompatible conditions for humans and marine life.

Therefore, there is a requirement to treat Rh B pollutants before discharge into the environment. Recently, numerous methods have been proposed to overcome environmental issues for a clean and balanced ecosystem. So there is a need to find a suitable solution to remove or degrade these organic dyes.

For this purpose, various processes like electrochemical, chemical precipitation, adsorption, photocatalysis, etc, have been used [7,8]. Over the last two decades, many adsorbents such as biopolymers, activated carbon, multi-walled carbon nanotubes, hydrogels, zeolites, and silica have been used extensively to remove dyes due to their porous nature [9-11]. Among several techniques, photocatalysis has become prominent due to low cost and using a green route by sunlight.

The metal oxides (MO) like TiO_2, CdS, and WO_3 and their composites have revealed a tremendous approach for the photocatalytic process for degrading organic dyes [12,13]. The main advantage of metal oxides is using solar energy (renewable energy source) to convert dyes into harmless products. However, the individual oxides have some limitations, i.e., large energy band gap and the fast recombination rate of charge carriers [14,15], which can be controlled by fabrication with other oxides or catalysts by making binary or ternary composites.

**Corresponding author: Muhammad Tariq*
Email address: mtnazir@yahoo.com
DOI: http://dx.doi.org/10.13171/mjc02302161680tariq

Received January 3, 2023
Accepted January 27, 2023
Published February 16, 2023

The nanocomposites can proficiently absorb sunlight and inhabit the recombination of e-/h + pairs that may work as an excellent photocatalyst [16]. The researchers have synthesized pure ZnO, WO_3- ZnO binary nanocomposites and studied their photocatalytic activity [17,18]. Patil et al. [19] have synthesized TiO_2-WO_3 binary composite and tested its photocatalytic activity on methyl red and congo red dyes under visible light. Sajjad et al.[20] have also prepared ZnO/WO3 nanocomposite using different concentrations of ZnO and tested its photocatalytic efficiency against MO dye, which was more significant compared to the pure WO_3 and ZnO.

MoO_3 is a wide band gap semiconductor having good energetic and electric properties [21]. However, its visible light harvesting ability is limited and has fast electron-hole pair recombination. Therefore, to improve its photocatalytic efficiency, it can be combined with other materials like g-C_3N_4 and rGO. The g-C_3N_4 has a small bandgap of 2.70 eV, resulting from the sp^2 hybridization of the carbon and nitrogen that form the π -conjugated graphitic planes, having comparable graphite structure [22]. It is well known that the materials with delocalized conjugated π structure have been confirmed to have high charge separation efficiency and low charge recombination rate [23]. The g-C_3N_4 has been known as a visible light photocatalyst because of its light-capturing ability, physio and photochemical stability and easily prepared economic material [24]. However, the poor electrical conductivity and small surface area posed serious problems limiting the electrocatalytic activity of g-C_3N_4-based materials. Moreover, the photocatalytic activity and electron transport between adjacent conjugated planes are adversely affected by the weak van der Waals interaction forces between the planes [25]. Aiming to improve visible light photocatalytic efficiency, rGO has been widely investigated. rGO is considered a promising candidate that can be combined with binary composite to satisfy both aspects of effective transfer of photoelectrons to avoid the recombination of electrons- holes and better absorption capacity of the catalytic system toward the pollutant or dye [26]. It can accept the electrons to avoid the recombination, provides a favorable absorption of dye through π– conjugation between the dye and aromatic regions of rGO, and maintains perfect mechanical performance to stabilize the catalysis [26]. Considering the pros and cons of three necessary materials, MoO_3, g-C_3N_4, and rGO, we have designed a ternary composite (g-C_3N_4-MoO_3/rGO), and its photocatalytic activity was determined in the degradation of Rh B dye.

2. Results and Discussion

2.1. FT-IR studies

The FT-IR spectra of g-C_3N_4, GO, MoO_3, g-C_3N_4-MoO_3 (binary composite), and g-C_3N_4-MoO_3/rGO (ternary composite) are represented in Figure 1. It has been observed that a sharp peak appeared at 803.52cm^{-1} that is assigned out of phase bending vibration mode of triazine units of g-C_3N_4. The characteristic peak of MoO_3 appeared at 988 cm^{-1}. The spectrum of graphene oxide exhibit many peaks at 1015 cm^{-1}, 1382 cm^{-1}, 2114 cm^{-1}, and 3268 cm^{-1} corresponding to the C-O, C-OH, C=C, and O-H bond, respectively. The binary composite g-C_3N_4-MoO_3 exhibits the characteristic peak of MoO_3 at 980 cm^{-1}. In the ternary composite g-C_3N_4-MoO_3/rGO, the peaks at 579.6 cm^{-1} and 889 cm^{-1} represent MoO_3, the peak at 807 cm^{-1} represent g-C_3N_4 while the peaks at 1842 cm^{-1} and 2041 cm^{-1} represent C=O and C=C in rGO. The appearance of all the related peaks in the g-C_3N_4-MoO_3/rGO spectrum confirmed the ternary composite synthesis.

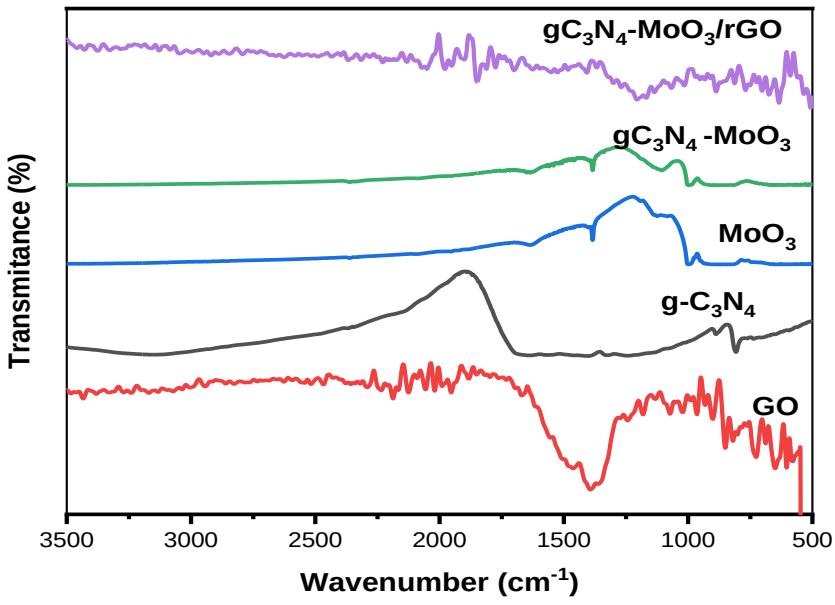

Figure 1. FT-IR spectra of GO, g-C_3N_4, MoO_3, g-C_3N_4-MoO_3 and g-C_3N_4-MoO_3/rGO

2.2. Powder XRD analysis

The XRD patterns of pure MoO_3, g-C_3N_4, and ternary composite g-C_3N_4-MoO_3/rGO are represented in Figure 2.

In ternary composite C_3N_4-MoO_3/rGO, all concerned peaks of g-C_3N_4 and MoO_3 were observed and compared with pure MoO_3 and g-C_3N_4. All the diffraction peaks of MoO_3 can be exactly indexed as the orthorhombic structure (JCPDF 35-0609) [27]. The main peaks of pure MoO_3 at 27.19°, 25.43°, and 23.11° correspond to the (021), (040), and (110) planes. On the other hand, the diffraction peaks of pure g-C_3N_4 appearing at 11.37 ° and 26.59° correspond to the (100) and (002) planes, which are assigned to the inter-layer structural packing and the interplanar stacking peaks of aromatic systems, respectively. The particle size of g-C_3N_4 and MoO_3 are 30 nm and 33 nm, respectively, as calculated using the Scherrer (Equation 1).

$$D=K\lambda/\beta.\ Cos\theta \quad (1)$$

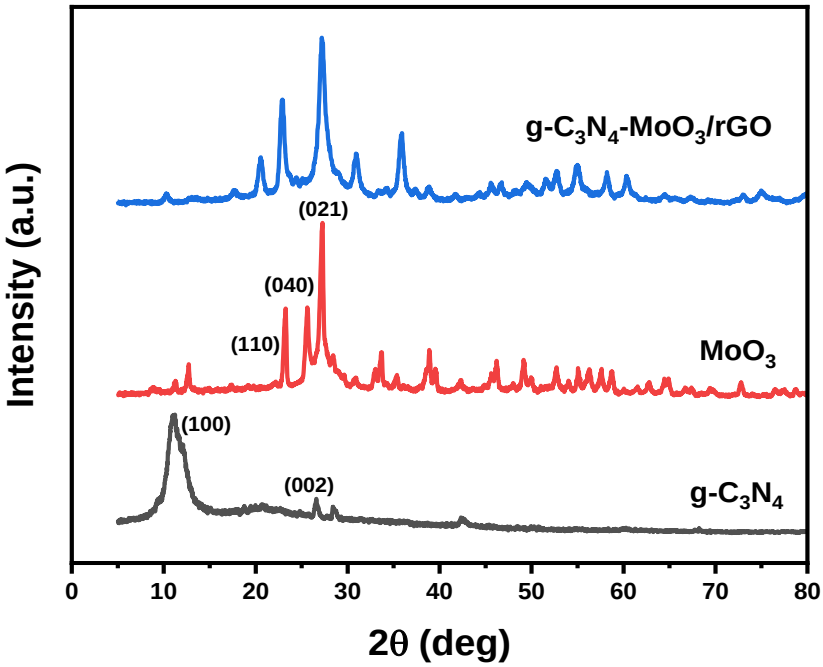

Figure 2. Powder XRD patterns of g-C_3N_4, pure MoO_3 and ternary composite (g-C_3N_4-MoO_3/rGO)

2.3. SEM analysis

SEM images of pure MoO_3 are represented in Figure 3a, which shows the small rod or tubular morphology of MoO_3 nanoparticles. In Figure 3b, it can be seen that agglomerated tubular MoO_3 nanoparticles are densely distributed into g-C_3N_4. There is an interfacial interaction between tubular MoO_3 nanoparticles and g-C_3N_4 particles which would enhance the separation of photogenerated carriers during degradation activity by shorting the transport distance [28]. A heterojunction structure is formed between MoO_3 crystalline and g-C_3N_4 layer. In Figure 3c, it has been observed that tubular MoO_3 nanoparticles are grown and merged into aggregated g-C_3N_4 and rGO.

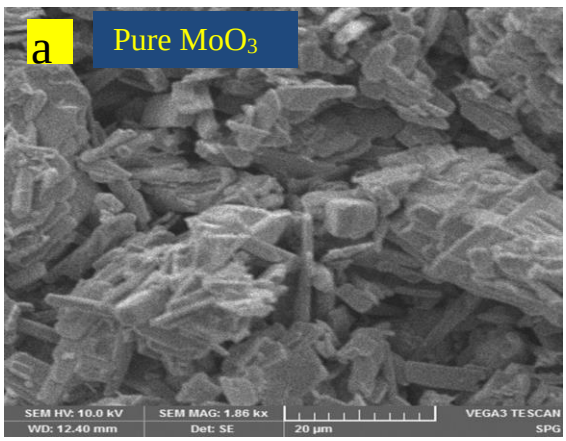

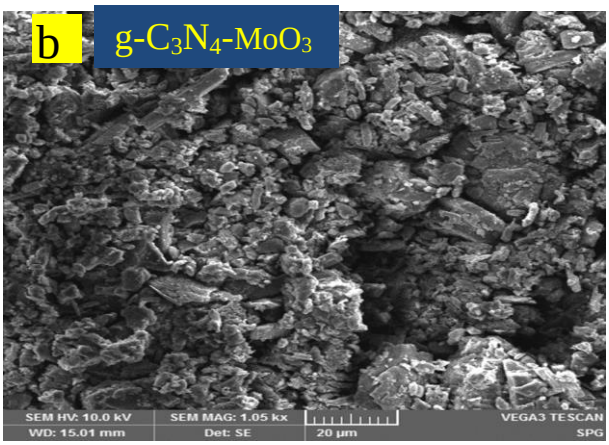

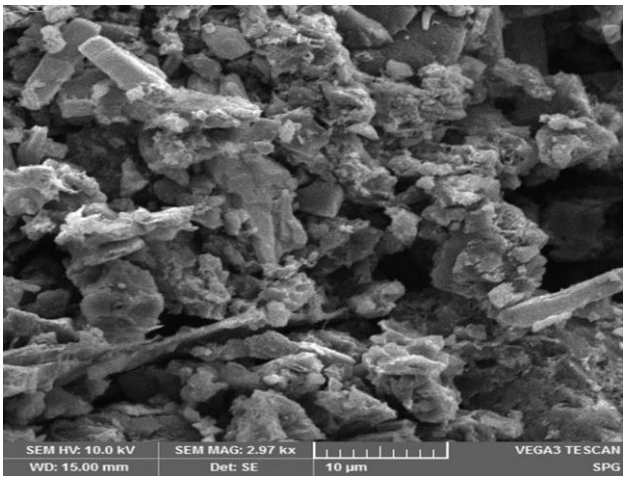

Figure 3. SEM images of (a) Pure MoO_3 (b) g-C_3N_4-$MoO_3$and g-C_3N_4-MoO_3/rGO

2.4. EDX (Energy dispersive X-ray) analysis

EDX was used to determine the elemental composition of pure MoO_3, binary composite g-C_3N_4-MoO_3, and ternary composite g-C_3N_4-MoO_3/rGO, and spectra are represented in Figure 4a-c, respectively. Mo is a prominent element, while Fe, P, Ni, and Al are also shown in the spectrum, but their composition is very close to 0.0 % . It may be due to improper cleaning of the stub. However the presence of 0.2 % of Na may be due to the precursor. The elemental composition of pure MoO_3, binary composite g-C_3N_4-MoO_3, and ternary composite g-C_3N_4-MoO_3/rGO is represented in Table 1. The pure MoO_3 showed 19.3 At % of Mo and 78.9 At % of oxygen.

The atomic percentage of other elements, C, N, and O, are also given in Table 1. The carbon atomic percentage was contributed from g-C_3N_4, while the oxygen atom was contributed from MoO_3 and a small percentage from rGO in the ternary composite. The overall At % of Mo, C, N & O confirmed the formation of g-C_3N_4-MoO_3 binary composites and ternary composite g-C_3N_4-MoO_3/rGO.

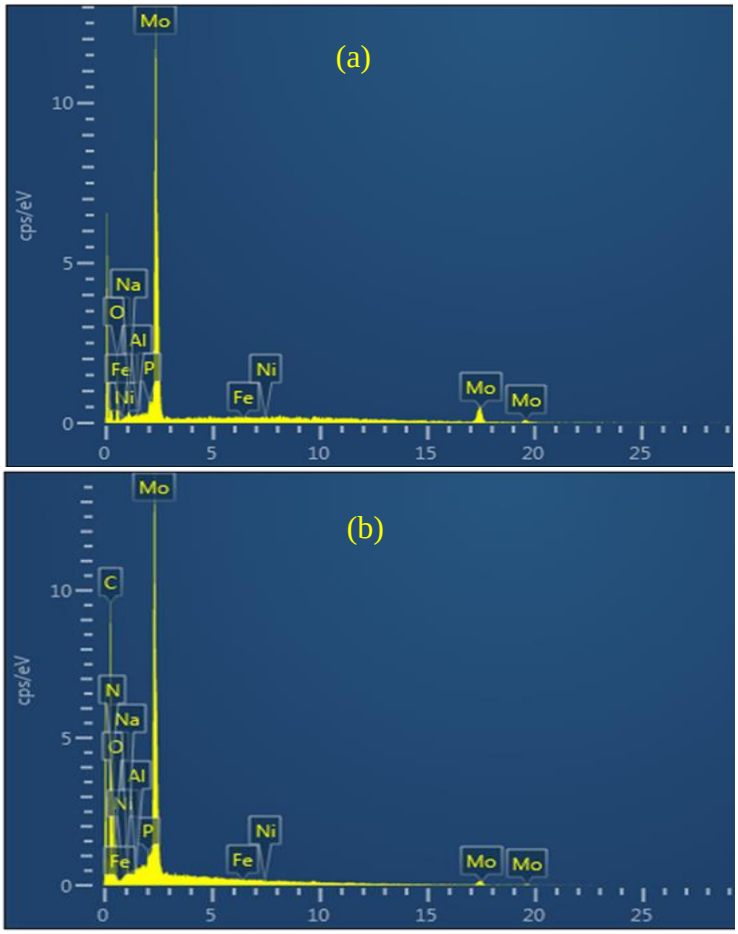

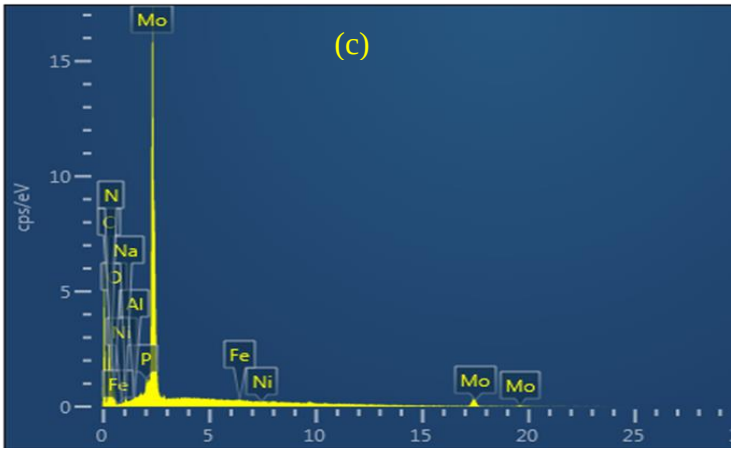

Figure 4. EDX Spectra (a) Pure MO_3 (b) g-C_3N_4-MO_3 and (c) g-C_3N_4-MO_3/rGO

Table 1. Elemental composition and atomic % of all the elements in the sample.

Elements	MoO_3	g-C_3N_4- MoO_3	g-C_3N_4-MoO_3/rGO
Atomic %			
C	**0.0**	**43.6**	**49.2**
N	0.0	43.8	37.3
O	78.9	10.7	9.2
Mo	19.3	1.8	4.1
Total	98.2	99.9	99.8

2.5. Photocatalytic degradation

The degradation property of ternary composite g-C_3N_4-MoO_3/rGO and all building precursors like MoO_3,g-C_3N_4, MoO_3/rGO,g-C_3N_4-MoO_3 was performed with Rhodamine B. The results are presented in Figure 5. The blank test with Rhodamine B dye was performed first, which resulted in no change in absorption, indicating the stability of the dye. Pure MoO_3 exhibited only 11% degradation efficiency, while g-C_3N_4 exhibited only 25% degradation efficiency. This may be due to poor absorbance activity and fast recombination of electron-hole pairs. The binary composite g-C_3N_4-MoO_3 and MoO_3/rGO showed comparatively better degradation efficiency of 55% and 58%, respectively. This may be due to poor absorbance activity and fast recombination of electron-hole pairs. The binary composite g-C_3N_4-MoO_3 and MoO_3/rGO showed comparatively better degradation efficiency of 55% and 58%, respectively. While ternary composite g-C_3N_4-MoO_3/rGO exhibited better degradation efficiency of 80%, which is more than some earlier reported studies, as shown in Table 2.

Table 2. Comparison of degradation efficiency with earlier reports.

Metal oxides	Efficiency %	Reference
WO3.NiO.ZnO	45.8%	[29]
WO3.NiO.ZnO/CNTs	66.19%	[29]
g-C_3N_4-MoO_3/rGO	80 %	Present study

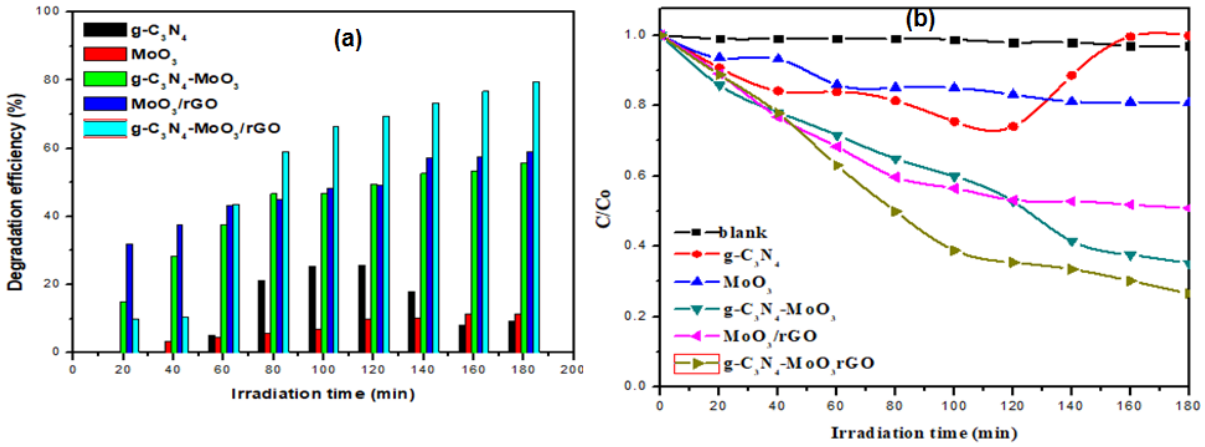

Figure 5. Degradation rate (a) and visible-light-driven photodegradation of Rhodamine B using g-C_3N_4, MoO_3, g-C_3N_4-WO_3, MoO_3/rGO, and g-C_3N_4-MoO_3/rGO

2.6. Proposed Mechanism for photodegradation

The photocatalytic activity of the semiconductor is influenced by the optical properties, including the energy level (valence and conduction band) of electronic bands and band gap. The general photocatalysis mechanism starts when light falls on the catalyst's surface. When light falls, three significant steps of photocatalysis occur; (i) e^- /h + pairs produced during the reaction (ii) deposition of charge carriers on the surface of photocatalyst (iii) oxidation and reduction of photogenerated electrons (e^-) and holes (h^+) at the surface of photocatalyst. The recombination rate of charge carriers is reduced by making a composite of MoO_3 with g-C_3N_4 and rGO. The proposed mechanism of degradation of Rh B is represented in Figure 6.

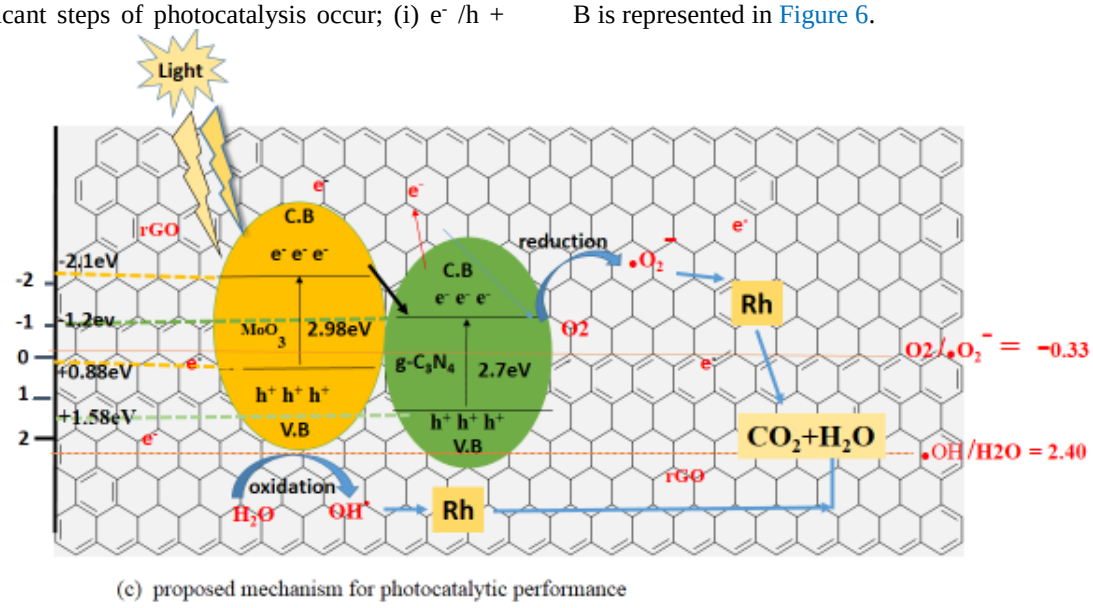

Figure 6. Proposed Mechanism of photocatalytic degradation of Rh-B

The CB edge and VB edge potentials of g-C_3N_4 and MoO_3 were calculated by using Equations (2) and (3) (Mulliken electronegativity theory) [30].

$$\mathbf{ECB = X - Ee - 0.5Eg} \quad (2)$$

$$\mathbf{EVB = ECB + Eg} \quad (3)$$

Where X is the electronegativity of the semiconductor calculated by the geometric mean of the electronegativity of the constituent atoms, Ee is the free electron energy on the hydrogen scale which is 4.5 eV, ECB, EVB, and Eg are respectively the conduction band, valence band, and energy gap potential..

The photoexcited e^- s from the conduction band of MoO_3 is migrated into V.B of g-C_3N_4 because MoO_3 has more significant C.B potential -2.1 than g-C_3N_4 (-1.12), simultaneously holes will be shifted from g-C_3N_4 to MoO_3. The electrons in the C.B of g-C_3N_4 oxidize the O_2 to yield $\cdot O_2^-$ while holes (h^+) reduce H_2O to produce · OH. These radicals ($\cdot O_2^-$, ·OH) then degrade the rhodamine dye to produce intermediates CO_2 and H_2O·

Oxidation Reactions

$$\mathbf{Photocatalyst \longrightarrow e^- + h^+}$$

$h^+ + H_2O \longrightarrow OH^{\cdot} + H^+$

$h^+ + OH^- \longrightarrow OH^{\cdot}$

$h^+ + \text{dye/pollutant} \; \text{dye}^{\cdot+} \longrightarrow \text{intermediates} \longrightarrow H_2O + CO_2$

Reduction Reactions

$e^- + O_2 \longrightarrow O_2^{\cdot-}$ (superoxide radicals)

$O_2^{\cdot-} + H^+ \longrightarrow HO_2^{\cdot}$

$HO_2^{\cdot} + HO_2^{\cdot} \longrightarrow H_2O_2 + O_2$

$e^- + H_2O_2 \longrightarrow OH^{\cdot} + OH^-$

Degradation involving Oxidation reactions of dye/pollutant

$OH^{\cdot} + \text{dye/pollutant} \longrightarrow \text{intermediates} \longrightarrow H_2O \text{ and } CO_2$

$O_2^{\cdot-} + \text{dye/ pollutant} \longrightarrow \text{intermediates} \longrightarrow H_2O \text{ and } CO_2$

3. Conclusion

The pue MoO_3, binary composite g-C_3N_4-MoO_3, and a ternary composite of g-C_3N_4-MoO_3/rGO was successfully prepared by ultrasonic wet impregnation method. The pure, binary, and ternary composite were analyzed for their preparation, structural and morphological analysis using various analytical tools. The photocatalytic activity of these prepared materials was assessed in the degradation of the organic pollutant Rhodamine B(Rh-B). The pure MoO_3 and g-C_3N_4 showed 11% and 25% degradation efficiency, respectively, which may be due to poor absorbance activity and fast recombination of electron-hole pair. While 55% and 58% degradation efficiency was obtained for binary g-C_3N_4-MoO_3 and MoO_3/rGO composite, respectively, due to synergistic effect. The ternary composite g-C_3N_4-MoO_3/rGO exhibited 80% degradation efficiency. The ternary composite showed better photo-degradation activity than pure and binary composite, possibly due to enhanced charge separation, smooth transfer of electrons, and low electron-holes recombination. Thus this study will contribute to the practical application of pollutant degradation.

Acknowledgements

The authors thank Bahauddin Zakariya University Multan, Pakistan, for financial support during the research.

4. Experimental

4.1. Graphite carbon nitride synthesis

The graphitic carbon nitride (g-C_3N_4) was prepared using the already reported procedure [28]. The method is briefly described as 4.0 g Melamine was taken in a corundum crucible and heated in a furnace at 500°C for 4 hours. Then it was cooled to room temperature. The yellow color product was obtained and ground to a fine powder.

4.2. Graphene oxide synthesis

The modified Hummer's method [31] was employed to synthesize graphene oxide. The method is briefly described as 1.0 g of crystalline graphite powder taken in a 500 mL beaker and then 45 mL conc. sulphuric acid was added. The reaction mixture was kept on stirring for 12 hours. After this, the reaction mixture was cooled by adding ice-cold water to about 12°C. Next, 3.0 g of $KMnO_4$ was added slowly, and the temperature was gradually increased to 35°C while stirring for two hours. Finally, the mixture was put in an ultrasonic bath for sonication for half an hour.

The obtained suspension was put on stirring again, and 100 mL of deionized water was added slowly. In the final step, H_2O_2 (6%) was placed into the above suspension until zero effervescence (bubbling due to exothermic reaction between H_2O_2 and $KMnO_4$) to stop the oxidation process as excess MnO_4- reduced to Mn_2^+. Finally, the product was obtained by centrifugation and washed many times with dilute HCl and deionized water to remove any remaining impurities. The obtained product was dried in an oven at 70°C overnight.

4.3. MoO_3 synthesis

MoO_3 nanoparticles were obtained using the hydrothermal process, as reported earlier [32]. First, 2.41 g of $Na_2MoO_4.2H_2O$ was dissolved in 45 mL of deionized water. Next, 2mL of 3 M HCl solution was added slowly into the sodium molybdate solution and stirred continuously until pH 2. Next, the clear solution was stirred for another 3 hrs. Then it was poured into a 100 mL Teflon-lined stainless steel autoclave and placed in an oven at 120°C for 18 hrs. The precipitated product was obtained by centrifugation and washed with deionized water and absolute ethanol many times to eliminate any present impurities. The product was then dried in an oven and calcined at 500°C for 2 hrs.

4.4. Binary composite g-C_3N_4-MoO_3 formation

g- C_3N_4-MoO_3 binary composite was obtained using ultrasonic-assisted wet impregnation method [31]. Briefly, 0.3g of MoO_3(30 wt%) was added into 40 mL mixture of ethanol and water (1:1 V ratio) and stirred for about 2 hrs. 0.7 g g-C_3N_4 (70 wt %) was added into the above suspension and kept on stirring and heating until the evaporation of the solvent. The solid product was then dried at 70ºC in an oven and calcined at 400°C for 1 hr in a muffle furnace.

4.5. Binary composite MoO_3/rGo formation

0.005 g graphene oxide (1.5 wt %) was added into 20 mL of ethanol: water (1:1 V ratio) and ultrasonicated for 1 hr. Then 0.3 g MoO_3 (30 wt%0 was added into the above suspension, stirred, and heated until dryness (evaporation of solvent). The

solid product was then dried at 70°C in an oven and calcined at 400°C for 1 hr in a muffle furnace.

4.6. Ternary composite g- C_3N_4-MoO_3/rGO

The g-C_3N_4-WO_3/rGO ternary composite was prepared by wet impregnation method [31]. First, 0.1 g graphene oxide solution was made by dissolving GO powder in 40 mL of a mixture of solvents (ethanol and deionized water in 1:1 V ratio and then sonicated for 1 hour. Then 0.3 g of MoO_3 (30 wt %) was added into the above solution and kept under stirring for 2 hours. Lastly 0.7g g-C_3N_4 (70 wt %) was added, and the whole mixture was stirred and heated slowly until the evaporation of the solvent. The resultant product was dried in an oven at 70°C and then calcined at 400°C for 1 hour to get the final ternary composite product.

4.7. Photocatalytic application in degradation of Rhodamine B

The g-C_3N_4-MoO_3/rGO catalytic application as a visible-light-driven catalyst was investigated in Rhodamine B (Rh-B) degradation. 200W bulb was used as a source of visible light. 10 ppm initial dye concentration was used. The pyrex reactor was 10 cm apart from the source of visible light. The dye degradation was observed using UV- a visible spectrophotometer (Shimadzu UV-1800) measuring the dye's change in absorbance (λmax) value. The sample aliquot was taken at regular intervals, and the degradation rate was recorded at λ_{max} of 554nm for Rh-B. First of all blank experiment without using a photocatalyst was performed in which 10 ppm of 100 mL dye solution was kept under the visible light source of a 200W bulb/xenon lamp, and absorbance was recorded. After the blank experiment, a 0.05g photocatalyst was added to 10 ppm of 100 mL dye solution. The solution was stirred in the dark for 30-60 minutes to establish and maintain absorption-desorption equilibrium. Then the reactor was illuminated using a 200W visible light source for a xenon lamp and allowed for the degradation process within the dye solution with a photocatalyst. After a regular time interval, a 4 mL sample solution was taken out of the reactor and centrifuged at 4500 rpm for about 5 minutes to separate the catalyst. Then absorbance was recorded in the visible range of 400-800nm. The degradation efficiency of composites was calculated by using the following formula;

Degradation (%) = (1- At/Ao) × 100

Where Ao = absorbance of dye at time = 0 min, At = absorbance of dye at time = t min.

References

1- M. Ismail, K. Akhtar, M. I. Khan, T. Kamal, M. A. Khan, M. Asiri, Abdullah, S. B. Khan, Pollution, Toxicity and Carcinogenicity of Organic Dyes and their Catalytic Bio-Remediation, Curr. Pharm. Des. **2019**, 25, 3645-3663.

2- S. Khan, A. Malik, Environmental and health effects of textile industry wastewater. In Environmental deterioration and human health. Springer, Dordrecht. **2014**, 55-71.

3- D. Suteu, C. Zaharia, A. Muresan, R. Muresan, A. Popescu, Using of industrial waste materials for textile waste water treatment, Environ. Eng. Manag J., **2009**, 8, 1097-1102.

4- M. K. Hussain, N. R. Khalid, M. Tanveer, I. Kebaili, H. Alrobei, Fabrication of CuO/MoO_3 pn heterojunction for enhanced dyes degradation and hydrogen production from water splitting, Int. J. Hydrogen Energy, **2022**, 47(34), 15491-15504.

5- L. Silva, B. Barrocas, M. M. Jorge, S. Serio, Photocatalytic Degradation of Rhodamine 6g Using Tio_2/wo_3 Bilayered Films Produced by Reactive Sputtering In Proceedings of the 6th International Conference on Photonics, Optics and Laser Technology (Photoptics), **2018**, 334-340.

6- N. R. Khalid, A. Arshad, M. B. Tahir, M. K. Hussain, Fabrication of p–n heterojunction Ag_2O@Ce_2O nanocomposites make enables to improve photocatalytic activity under visible light, Appl. Nanosci., **2021**, 11, 199-206.

7. M. Neelavannan, M. Revathi, C. A. Basha, Photocatalytic and electrochemical combined treatment of textile wash water, J. Hazard. Mater., **2007**, 149(2), 371-378.

8- Y. Anjaneyulu, N. S. Chary, D. S. S. Raj, Decolourization of industrial effluents–available methods and emerging technologies–a review, Rev. Environ. Sci. Biotechnol., **2005**, 4(4), 245-273.

9- M. Athari, M. Fattahi, M. Khosravi-Nikou, A. Hajhariri, Adsorption of different anionic and cationic dyes by hybrid nanocomposites of carbon nanotube and graphene materials over UiO-66, Sci. Rep., **2022**, 12(1), 20415.

10- S. Soleimani, A. Heydari, M. Fattahi, A. Motamedisade, Calcium alginate hydrogels reinforced with cellulose nanocrystals for methylene blue adsorption: Synthesis, characterization, and modeling, Ind. Crops Prod., **2023**, 192, 115999.

11- S. Soleimani, A. Heydari, M. Fattahi, Isolation and Characterization of Cellulose Nanocrystals from Waste Cotton Fibers Using Sulfuric Acid Hydrolysis, Starch-Stärke, 2022, 74(11), 2200159.

12- N. R. Khalid, M. K. Hussain, G. Murtaza, M. Ikram, M. Ahmad, A. Hammad, A novel Ag 2 O/Fe–TiO 2 photocatalyst for CO_2 conversion into methane under visible light, J. Inorg. Organomet. Polym. Mater., **2019**, 29, 1288-96.

13- M. K. Hussain, N. R. Khalid, Surfactant-assisted synthesis of MoO_3 nanorods and its application in photocatalytic degradation of different dyes in an aqueous environment, J. Mol. Liq., **2022**, 346, 117871.

14- T. Munawar, F. Mukhtar, M. S. Nadeem, M. Asghar, K. Mahmood, A. Hussain, F. Iqbal, Multifunctional properties of Zn0· 9Mn0. 05M0. 05O (M= Al, Bi, Sr, Ag) nanocrystals-structural and optical study: Enhance sunlight driven photocatalytic activity, Ceram. Int., **2020**, 46(14), 22345-22366.

15- S. Yasmeen, T. Munawar, M. Asghar, M. A. Khan, A. Hussain, F. Iqbal, Synthesis and photocatalytic study of Zn0. 90Co0. 10O and Zn0. 90Co0. 05M0. 05O (M= Ca, Ba, Cr, Pb) nanocrystals: structural, optical and electrical investigations, J. Mater. Res. Technol., **2020**, 9(3), 4076-4096.

16- R. Gusain, K. Gupta, P. Joshi, O. P. Khatri, Adsorptive removal and photocatalytic degradation of organic pollutants using metal oxides and their composites: A comprehensive review, Adv. Colloid Interface Sci., **2019**, 272, 102009.

17- S. S. P. Selvin, A. G. Kumar, L. Sarala, R. Rajaram, A. Sathiyan, J. Princy Merlin, I. S. Lydia, Photocatalytic degradation of rhodamine B using zinc oxide activated charcoal polyaniline nanocomposite and its survival assessment using aquatic animal model, ACS Sustain. Chem. Eng., **2018**, 6(1), 258-267.

18- J. Xie, Z. Zhou, Y. Lian, Y. Hao, X. Liu, M. Li, Y. Wei, Simple preparation of WO_3–ZnO composites with UV–Vis photocatalytic activity and energy storage ability, Ceram. Int., **2014**, 40(8), 12519-12524.

19- S. M. Patil, S. P. Deshmukh, K. V. More, V. B. Shevale, S. B. Mullani, A. G. Dhodamani, S. D. Delekar, Sulfated TiO_2/WO_3 nanocomposite: An efficient photocatalyst for degradation of Congo red and methyl red dyes under visible light irradiation, Mater. Chem. Phys., **2019**, 225, 247-255.

20- A. K. L. Sajjad, S. Sajjad, A. Iqbal, ZnO/WO_3 nanostructure as an efficient visible light catalyst, Ceram. Int., **2018**, 44(8), 93649371.

21- A. Chithambararaj, N.S. Sanjini, S. Velmathi, A.C. Bose, Preparation of h-MoO_3 and a-MoOnanocrystals: a comparative study on photocatalytic degradation of methylene blue under visible light irradiation, Phys. Chem. Chem. Phys., **2013**, 15, 14761.

22- J. R. Holst, E. G. Gillan, Fromtriazines to heptazines: deciphering the local structure of amorphous nitrogen-rich carbon nitride materials, J. Am. Chem. Soc., **2008**, 130(23), 7373-7379.

23- Y. Zhang, T. Mori, L. and J. Ye. Niu, Non-covalent Doping of Graphitic Carbon Nitride Polymer with Graphene: Controlled Electronic Structure and Enhanced Optoelectronic Conversion, Energ. Environ. Sci., **2011**, 4, 4517.

24- Y. Li, H. Zhang, P. Liu, D. Wang, Y. Li, H. Zhao, Cross-linked g-C_3N_4/rGOnanocomposites with tunable band structure and enhanced visible light photocatalytic activity. Small, **2013**, 9(19), 3336-3344.

25- X. Wang, X. Chen, A. Thomas, X. Fu, M. Antonietti, Metal-containing carbon nitride compounds: a new functional organic–metal hybrid material, Adv. Mater., **2009**, 21(16), 1609-1612.

26- G. Jiang, Z. Lin, C. Chen, L. Zhu, Q. Chang, N. Wang, H. Tang, TiO_2 nanoparticles assembled on graphene oxide nanosheets with high photocatalytic activity for removal of pollutants, Carbon, **2011**, 49(8), 2693-2701.

27- L. Huang, H. Xu, R. Zhang, X. Cheng, J. Xia, Y. Xu, &H. Li, Synthesis and characterization of g-C_3N_4/MoO_3 photocatalyst with improved visible-light photoactivity, Appl. Surface Sci., **2013**, 283, 25-32.

28- I. Aslam, C. Cao, M. Tanveer, W. S. Khan, M. Tahir, M. Abid, N. Mahmood, a synergistic effect between WO_3 and g C_3N_4 towards efficient visible-light-driven photocatalytic performance, New J. Chem. **2014**, 38(11), 5462-5469.

29- M. A. Butler, D. S. Ginley, Prediction of flat band potentials at semiconductor-electrolyte interfaces from atomic electronegativities, J. Electrochem. Soc., **1978**, 125(2), 228.

30- Y. Xu, M. A. Schoonen, The absolute energy positions of conduction and valence bands of selected semiconducting minerals, Am. Mineral., **2000**, 85(3-4), 543-556.

31- H. Y. Hafeez, S. K.Lakhera, S. Bellamkonda, G. R. Rao, M. V. Shankar, D. W. Bahnemann, B. Neppolian, Construction of ternary hybrid layered reduced graphene oxide supported g-C_3N_4-TiO_2 nanocomposite and its photocatalytic hydrogen production activity, Int. J. Hydrogen Energy, **2018**, 43(8), 3892-3904.

32- S. Dutta, Pal, S. De, One-dimensional α-MoO_3 nanorods for high energy density pseudocapacitor, paper presented at the AIP Conference Proceedings, **2018,** 1942, 140086.